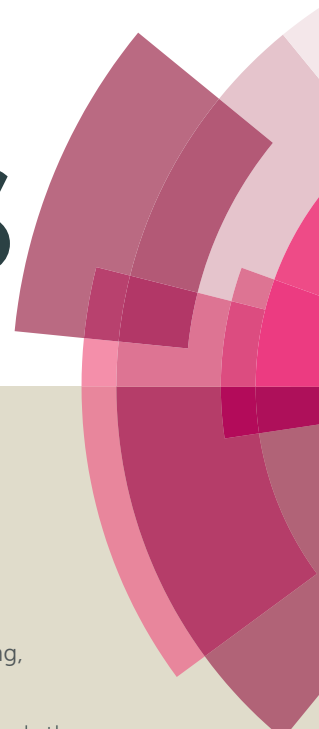


RSC Advances



This article can be cited before page numbers have been issued, to do this please use: K. Song, X. Meng, J. Zhang, Y. Zhang, X. Wang and J. Zhu, *RSC Adv.*, 2016, DOI: 10.1039/C6RA23196A.



This is an *Accepted Manuscript*, which has been through the Royal Society of Chemistry peer review process and has been accepted for publication.

Accepted Manuscripts are published online shortly after acceptance, before technical editing, formatting and proof reading. Using this free service, authors can make their results available to the community, in citable form, before we publish the edited article. This *Accepted Manuscript* will be replaced by the edited, formatted and paginated article as soon as this is available.

You can find more information about *Accepted Manuscripts* in the [Information for Authors](#).

Please note that technical editing may introduce minor changes to the text and/or graphics, which may alter content. The journal's standard [Terms & Conditions](#) and the [Ethical guidelines](#) still apply. In no event shall the Royal Society of Chemistry be held responsible for any errors or omissions in this *Accepted Manuscript* or any consequences arising from the use of any information it contains.



RSC Advances

PAPER

A simple grinding-calcination approach to prepare $\text{Co}_3\text{O}_4\text{-In}_2\text{O}_3$ heterojunction structure with high-performance gas-sensing property to ethanol

Kai Song, Xiaoqian Meng, Jianli Zhang, Yue Zhang, Xin Wang, Junwu Zhu*

Received 00th January 20xx,
Accepted 00th January 20xx

DOI: 10.1039/x0xx00000x

www.rsc.org/MaterialsA

Developing gas sensing devices with high sensitivity, good selectivity and excellent stability is becoming more and more important as the toxic or harmful gases are threatening human health. Herein, we report a simple grinding-calcination method to prepare high-performance gas sensing materials based on a novel $\text{Co}_3\text{O}_4\text{-In}_2\text{O}_3$ heterojunction structure. Especially, the morphological and structural analyses indicate that the n-type In_2O_3 and p-type Co_3O_4 semiconductors are successfully combined and form stable heterojunction structure only through a simple grinding-calcination process. In which, electrons would transfer from n-type In_2O_3 to p-type Co_3O_4 and then combine with holes belongs to Co_3O_4 nanoparticles, which can explain the formation mechanism of electron depletion layer or the unique heterojunction structure. Interestingly, the sensing materials based on $\text{Co}_3\text{O}_4\text{-In}_2\text{O}_3$ heterojunction exhibit excellent sensing properties to ethanol. The enhanced sensing performance can be attributed to the electron depletion layer formed at interface between n-type In_2O_3 and p-type Co_3O_4 . Particularly, the sensing device based on $\text{Co}_3\text{O}_4\text{-In}_2\text{O}_3$ heterojunction structure with 1 wt% Co_3O_4 (labeled as $\text{Co}_3\text{O}_4\text{-In}_2\text{O}_3$ (1%)) in the composite systems shows greatly high gas response to ethanol (approximately 62.13 at 240 °C, 1.36 times higher than pure In_2O_3 and 11.4 times higher than pure Co_3O_4). Moreover, the $\text{Co}_3\text{O}_4\text{-In}_2\text{O}_3$ (1%) sensing device shows extremely low detection limitation to ethanol (the gas response value can reach up to 4.4 to 5 ppm of ethanol, which is 1.43 times higher than that of pure In_2O_3). Moreover, the fast response and recover time (42 and 92 s, respectively), high selectivity and high stability presented by $\text{Co}_3\text{O}_4\text{-In}_2\text{O}_3$ heterojunction holds a great promise for design of excellent gas sensing materials for practical gas detection.

Introduction

As we know, environmental pollution is threatening human beings health. With the increasing concerns of controlling air pollution and detecting noxious gas, gas sensing devices have been extensively studied in recent years. Up to now, various materials have been used to fabricate sensing devices, such as metal-organic complexes,¹ graphene oxide,² and metal oxides.³ Among these, metal oxide semiconductors such as SnO_2 ,⁴⁻⁶ ZnO ,⁷⁻⁹ In_2O_3 ,^{10,11} Co_3O_4 ^{12,13} have attracted significant interest due to their high sensitivity, low detection limits, high stability and low cost.^{14,15}

Indium oxide (In_2O_3) is an important n-type semiconductor of the above metal oxide semiconductors. It has been reported to exhibit high sensitivity, selectivity, and stability to many different types of volatile organic compounds (VOCs) or noxious gases.¹⁶⁻²⁰ Especially, sensing devices based on In_2O_3

semiconductor have great advantages in detecting ethanol owing to its wide bandgap ($E_g=3.55\text{-}3.75\text{ eV}$)²¹⁻²³. In order to further improve the sensing performance of traditional materials, a variety of methods have been employed to improve the sensing properties of gas sensing devices based on In_2O_3 semiconductor in the last few years. For example, Gai *et al.* prepared nitrogen-doped indium oxide nanocrystals, which showed higher sensing properties to ethanol.²⁴ Wang *et al.* synthesized novel Ag-loaded In_2O_3 hierarchical nanostructures, presenting greatly enhanced sensing performances to methanol.²⁵ Besides, Singh *et al.* found that the sensitivity towards different reducing gases could be improved by combining In_2O_3 nanowires and ZnO shell layers.²⁶ However, when it comes to practical application, there are still some deficiencies. For example, much more factors which refer to low detecting limitation, simplicity in manufacture process, and low cost should be taken into consideration in the development of practical gas sensing devices. Therefore, it is extremely essential to develop a more efficient system to help meet the growing demands of fabricating high-performance sensing devices based on In_2O_3 semiconductor.

In fact, the concept of combining n- and p-type semiconductors to fabricate gas sensing materials has been widely accepted. The gas sensing properties would be

Key Laboratory for Soft Chemistry and Functional Materials, Ministry of Education, Nanjing University of Science and Technology, Nanjing 210094, China. E-mail: zhujw@njust.edu.cn

Electronic Supplementary Information (ESI) available: [The other XRD, TEM and sensing response data]. See DOI: 10.1039/x0xx00000x

improved because of the synergistic effect of n- and p-type semiconductors.²⁷⁻²⁹ As an important p-type semiconductor, cobaltic oxide (Co_3O_4) with a bandgap of 2.2 eV¹⁵ can form stable heterojunction with n-type In_2O_3 . Actually, the Co_3O_4 - In_2O_3 heterojunction structure has been reported in the past few years.³⁰⁻³³ However, until now, to the best knowledge of the authors, few studies about gas sensing devices based on Co_3O_4 - In_2O_3 heterojunction structure were reported. Furthermore, many reported synthesis processes of heterojunction structure are complicated. Therefore, developing a convenient method for preparing Co_3O_4 - In_2O_3 heterojunction structure with excellent gas-sensing properties is highly desirable.

Herein, we reported a simple method to synthesize Co_3O_4 - In_2O_3 nanoparticles with heterojunction structure. This novel gas sensing material has been confirmed to have superior sensing properties to ethanol. Moreover, the higher response value of sensing devices assembled in this work can better satisfy modern detecting process than those sensing devices based on pure In_2O_3 semiconductor. Besides, there are some other superior performances have been discovered such as low detection limitation, short response and recover times, and high selectivity. In general, sensing devices based on Co_3O_4 - In_2O_3 heterojunction structure are more accordant with practical application compared with those other similar materials. We believe that the unique heterojunction structure would have great advantage in gas detection.

Experimental section

Synthesis of Co_3O_4 - In_2O_3 heterojunction structure

All the chemicals used in the experiments were in analytic grade and used without further purification. Co_3O_4 - In_2O_3 nanoparticles with heterojunction structure were fabricated by a grinding-calcination process using $\text{In}(\text{NO}_3)_3 \cdot 4.5\text{H}_2\text{O}$ and $\text{Co}(\text{NO}_3)_2 \cdot 6\text{H}_2\text{O}$ as the starting materials. In a typical procedure, 2 mmol $\text{In}(\text{NO}_3)_3 \cdot 4.5\text{H}_2\text{O}$ were transferred into an agate mortar with different contents of $\text{Co}(\text{NO}_3)_2 \cdot 6\text{H}_2\text{O}$ (0.5, 1, 2, 5, 10 wt% of mass of $\text{In}(\text{NO}_3)_3 \cdot 4.5\text{H}_2\text{O}$). The mixture was ground for 30 mins to make the two reagents mixed evenly. Next, the obtained mixture was accomplished by calcination at 450 °C for 2 h under an air atmosphere with a heating rate of 1 °C/min, forming the Co_3O_4 - In_2O_3 heterojunction structure. Similarly, pure In_2O_3 and Co_3O_4 nanoparticles were respectively fabricated through a similar procedure for further analyses.

Characterization

Powder X-ray diffraction (XRD) analyses were performed on a Bruker D8 Advance diffractometer with $\text{Cu K}\alpha$ radiation ($\lambda = 1.54 \text{ \AA}$). Raman measurements were tested by a Renishaw Raman microscope with a 514.5 nm wavelength as incident laser. The elemental compositions of samples were analyzed by a PHI QUANTERA II X-ray photoelectron spectrometer (XPS), using monochromatic $\text{Al K}\alpha$ radiation as the exciting source (energy resolution < 0.60 eV). The morphologies of as-

obtained products were observed on a transmission electron microscope (TEM, JEOL JEM-2100) and scanning electron microscope (SEM, JEOL JSM-7001F). The thermogravimetric analyzer (TGA) was carried out using a DTG-60 (Shimadzu Corporation, Japan) in air atmosphere, and the samples were heated from 25 to 450 °C at a heating rate of 20 °C/min.

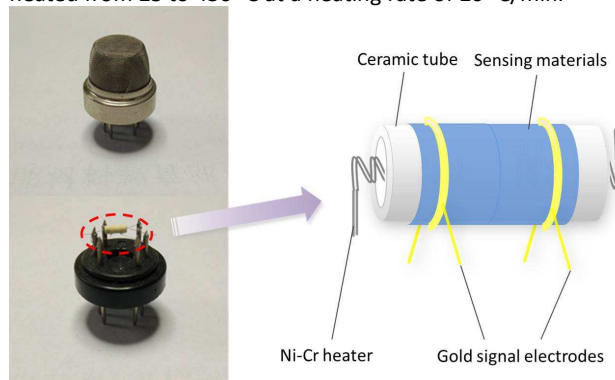


Fig. 1 The photo and schematic illustration of the sensing device.

Fabrication and measurement of gas sensors

The gas-sensing properties of as-prepared Co_3O_4 - In_2O_3 heterojunction structure were performed on a WS-30A measuring system (Winsen Electronics Co. Ltd.) under static testing conditions. The detailed fabrication and testing processes of sensing devices were shown as follows. Firstly, the as-prepared powder was mixed with several drops of deionized water to form uniform slurry through slight milling. The resulting paste was then coated onto a ceramic tube (1 mm in diameters and 4 mm in lengths), which was positioned with gold electrodes and platinum conducting wires. A Ni-Cr heating wire was put through the ceramic tube to supply different operating temperatures, which could be controlled in the range of 100 to 400 °C by tuning the heating voltage. Finally, the ceramic tube was welded onto a six-probe pedestal which was plugged into a measurement board of the sensor measuring system. The photo and schematic illustration of sensing devices were presented in Fig. 1. Before testing, the sensing devices were aged in air for 12 h at 300 °C for the purpose of eliminating deionized water and improving stability. After that, the obtained sensing devices were placed in gas chamber, where different concentrations of detected gas could be introduced with a microsyringe. The gas-sensing sensitivity of sensing devices is defined as $S = R_a/R_g$, where R_a and R_g are the electrical resistance of sensor in air and in detected gas at operating temperatures, respectively.³⁴ The response time is defined as the time for sensor resistance to reach 90 % of the equilibrium value following a step increase in the target gas concentration, whereas the recovery time is defined as the time necessary for the sample to return to 10 % above the original sensor resistance in air after removing the target gas.³⁵

Results and discussion

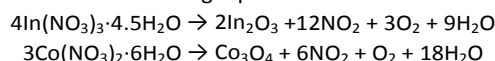
Structure and Morphology of $\text{Co}_3\text{O}_4\text{-In}_2\text{O}_3$ heterojunction structure

The crystal structure of prepared samples was characterized by XRD. As shown in Fig. 2a, the sharp diffraction peaks indicate high crystallinity of $\text{Co}_3\text{O}_4\text{-In}_2\text{O}_3$ (1 %) nanoparticles. The characteristic peaks at $2\theta = 21.50^\circ, 30.58^\circ, 35.47^\circ, 45.69^\circ, 51.04^\circ$ and 60.68° can be explicitly indexed to (211), (222), (400), (431), (440) and (622) crystal planes of cubic phase of In_2O_3 (JCPDS no. 04-0614), respectively. In addition, no characteristic peaks of impurities such as $\text{In}(\text{NO}_3)_3$ or $\text{Co}(\text{NO}_3)_2$ are observed. Nevertheless, it cannot be neglected that no typical diffraction peaks of Co_3O_4 are observed in the XRD pattern of $\text{Co}_3\text{O}_4\text{-In}_2\text{O}_3$ (1 %), which could be attributed to the lower content and crystallinity of Co_3O_4 compared with In_2O_3 . Therefore, the XRD analysis of samples prepared by calcining pure $\text{Co}(\text{NO}_3)_2 \cdot 6\text{H}_2\text{O}$ was also performed to prove the existence of Co_3O_4 . Obviously, as shown in Fig. 2a, the characteristic peaks at $2\theta = 31.27^\circ, 36.85^\circ, 44.81^\circ, 59.35^\circ$ and 65.23° can be indexed to (220), (311), (400), (511) and (440) crystal planes of cubic phase of Co_3O_4 (JCPDS no. 43-1003), respectively. More XRD patterns of $\text{Co}_3\text{O}_4\text{-In}_2\text{O}_3$ nanoparticles with different contents of Co_3O_4 (0, 0.5, 2, 5, 10 wt%) were also performed (Fig. S1, Supporting Information). Similarly, it's still hard to distinguish typical diffraction peaks of Co_3O_4 . Nevertheless, we can find that the intensity of In_2O_3 diffraction peaks decrease and the diffraction peaks become wider with the contents of Co_3O_4 increasing from 0 to 10 wt %, which further confirm the existence of Co_3O_4 .

The Raman spectrum analysis was also investigated. Fig. 2b shows the Raman curves of pure In_2O_3 , $\text{Co}_3\text{O}_4\text{-In}_2\text{O}_3$ (1 %) and $\text{Co}_3\text{O}_4\text{-In}_2\text{O}_3$ (10 %). According to previous reports, the peaks observed at 131.7, 309.1, 498.5 and 630.3 cm^{-1} are in agreement with In_2O_3 characteristic peaks, while the peaks observed at 479.1, 516.6, 687.2 cm^{-1} are in agreement with Co_3O_4 characteristic peaks.³⁶⁻³⁸ From the Raman pattern of $\text{Co}_3\text{O}_4\text{-In}_2\text{O}_3$ (1 %), the characteristic peaks of both Co_3O_4 and In_2O_3 can be observed. However, the intensity of Co_3O_4 characteristic peaks is still weak. So the Raman measurement of $\text{Co}_3\text{O}_4\text{-In}_2\text{O}_3$ (10 %) was also performed to further confirm the existence of Co_3O_4 . It is noteworthy that the intensity of Co_3O_4 characteristic peaks is greatly enhanced when the contents of Co_3O_4 increase from 1 to 10 %, whereas the intensity of In_2O_3 characteristic peaks is getting weaker. As a result, the Raman patterns can also demonstrate the existence of Co_3O_4 .

To further confirm the element composition of $\text{Co}_3\text{O}_4\text{-In}_2\text{O}_3$ (1 %) nanoparticles, the XPS analysis was also performed. In Fig. 2c, the characteristic peaks of In, O, Co, C can be observed without any other impurity elements. Similarly, the peak intensity of Co is obviously weaker than other elements because of the low content of Co in $\text{Co}_3\text{O}_4\text{-In}_2\text{O}_3$ (1 %), which agrees well with the XRD results. The In 3d spectrum (Fig. 2d) exhibits a $3d_{5/2}$ peak at 443.5 eV, $3d_{3/2}$ peak at 451.0 eV,³⁹ which confirms the presence of In_2O_3 . The presence of Co 2p showed in Fig. 2e further demonstrates the successful introduction of small quantity of Co_3O_4 . The characteristic peaks at 794.2 and 779.0 eV with a spin-energy separation of 15.2 eV correspond to Co $2p_{1/2}$ and Co $2p_{3/2}$, respectively, which are characteristic of a Co_3O_4 phase.⁴⁰

To simulate the thermal decomposition process of the reactants, the TGA of $\text{In}(\text{NO}_3)_3 \cdot 4.5\text{H}_2\text{O}$ and $\text{Co}(\text{NO}_3)_2 \cdot 6\text{H}_2\text{O}$ was also performed. As we can see from Fig. 2f, $\text{In}(\text{NO}_3)_3 \cdot 4.5\text{H}_2\text{O}$ and $\text{Co}(\text{NO}_3)_2 \cdot 6\text{H}_2\text{O}$ start to lose crystal water at 56 and 47°C , respectively. Shortly afterwards, $\text{In}(\text{NO}_3)_3$ and $\text{Co}(\text{NO}_3)_2$ start to decompose at 161 and 196°C , respectively. Finally, $\text{In}(\text{NO}_3)_3$ and $\text{Co}(\text{NO}_3)_2$ are fully decomposed to In_2O_3 and Co_3O_4 at 247 and 252°C . The equations of decomposition reaction in air can be inferred as the following equations.



Combining the equations and TGA patterns, it is found that each phase of these two thermal decomposition curves matches well with theoretical calculation of the weight change. Moreover, no other changes can be observed when the temperature keeps rising to 450°C . In general, the TGA patterns can further confirm the type of our products after calcination process and demonstrate reaction process as well.

The morphologies of as prepared $\text{Co}_3\text{O}_4\text{-In}_2\text{O}_3$ nanoparticles were investigated by TEM and SEM. As shown in Fig. 3a, it is clear to see that the $\text{Co}_3\text{O}_4\text{-In}_2\text{O}_3$ (1 %) nanoparticles are composed of irregular secondary particles after calcinations process. The inset of Fig. 3a reports a size distribution of obtained $\text{Co}_3\text{O}_4\text{-In}_2\text{O}_3$ (1 %) nanoparticles, which indicates that the diameters of these nanoparticles are ranging from a few tens of nanometers to about 500 nanometers. In Fig. 3b, we

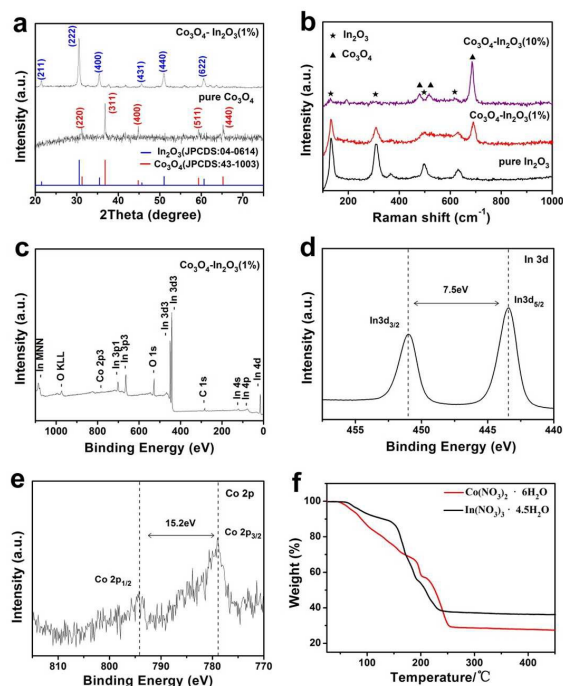


Fig. 2 (a) XRD patterns of $\text{Co}_3\text{O}_4\text{-In}_2\text{O}_3$ (1 %) and pure Co_3O_4 ; (b) Raman patterns of pure In_2O_3 , $\text{Co}_3\text{O}_4\text{-In}_2\text{O}_3$ (1 %) and $\text{Co}_3\text{O}_4\text{-In}_2\text{O}_3$ (10 %); XPS survey of whole scan spectrum (c), In 3d of $\text{Co}_3\text{O}_4\text{-In}_2\text{O}_3$ (1 %) (d) and Co 2p of $\text{Co}_3\text{O}_4\text{-In}_2\text{O}_3$ (1 %) (e); (f) TGA patterns of $\text{In}(\text{NO}_3)_3 \cdot 4.5\text{H}_2\text{O}$ and $\text{Co}(\text{NO}_3)_2 \cdot 6\text{H}_2\text{O}$.

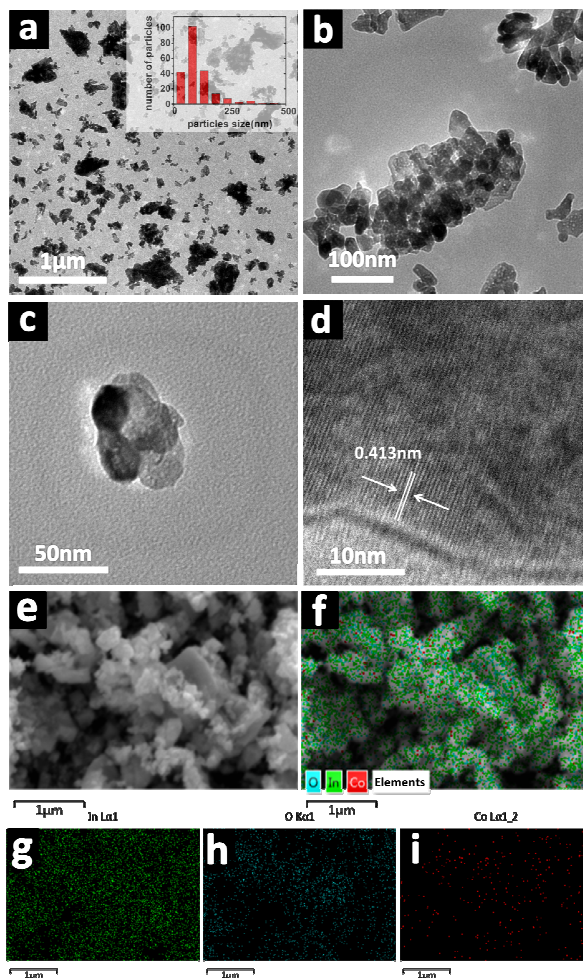


Fig. 3 TEM (a-d) and SEM (e, f) images of $\text{Co}_3\text{O}_4\text{-In}_2\text{O}_3$ (1 %) nanoparticles; (g-i) elemental mapping images of In, O, and Co respectively of the $\text{Co}_3\text{O}_4\text{-In}_2\text{O}_3$ (1 %).

can clearly see that the irregular secondary particles consist of primary particles with sizes of dozens of nanometers. Besides, we believe that tiny holes formed between the primary particles have great advantages in gas transmission. Nevertheless, it is still hard to distinguish Co_3O_4 nanoparticles from the composite system. This can be attributed to low content of Co_3O_4 and the tight combination of Co_3O_4 and In_2O_3 nanoparticles after high temperature calcination. The TEM images of pure In_2O_3 and pure Co_3O_4 can be seen in Fig. S2. It can be seen that the diameters of pure Co_3O_4 particles are about 30 to 50 nm. The small size and low content of pure Co_3O_4 nanoparticles make it more difficult to distinguish Co_3O_4 nanoparticles from the heterojunction structure. Moreover, from the HRTEM image of $\text{Co}_3\text{O}_4\text{-In}_2\text{O}_3$ (1 %) nanoparticles (Fig. 3d) (taken from the single particle in Fig. 3c), the lattice spacing of 0.413 nm can be assigned to the (211) plane of cubic phase of In_2O_3 . The legible lattice spacing indicates high degree of crystallinity, which matches well with the XRD analysis. The SEM images of as-synthesized $\text{Co}_3\text{O}_4\text{-In}_2\text{O}_3$ (1 %) nanoparticles can be seen in Fig. 3e and f. It can be visually

observed that the composite consists of nanoparticles with irregular diameters. Moreover, the spatial distribution of different compositional elements is clarified by the elemental mapping of In, O, and Co, respectively (Fig. 3g-i). As expected, the distribution of these three elements is homogeneous, which indicates the successful introduction of Co_3O_4 nanoparticles in composite systems.

Gas Sensing Performances

Ethanol is a widely used reagent in industries and labs, and it is necessary to fabricate one kind of efficient, inexpensive gas sensing device for ethanol detecting. Accordingly, the obtained $\text{Co}_3\text{O}_4\text{-In}_2\text{O}_3$ heterojunction structure was fabricated as gas sensing device, and its gas sensing performance was explored. As we know, the operating temperature can greatly influence the sensing properties. Therefore, the gas sensing devices fabricated in this work were investigated towards 100 ppm of ethanol at different temperatures ranging from 160 to 400 °C (Fig. 4a). It is evident that the responses of pure In_2O_3 , $\text{Co}_3\text{O}_4\text{-In}_2\text{O}_3$ (1 %), and $\text{Co}_3\text{O}_4\text{-In}_2\text{O}_3$ (10 %) towards 100 ppm ethanol first increase with rising operating temperatures and reach its maximum at 240 °C, and then sharply decrease with further increasing temperatures. This result can be ascribed to the kinetics and thermodynamics of gas adsorption and desorption on the surfaces of $\text{Co}_3\text{O}_4\text{-In}_2\text{O}_3$ heterojunction structure or other similar semiconducting metal oxides.^{18, 41} Actually, when the sensing devices are exposed to ethanol vapor, the ethanol molecules would be adsorbed on active sites on the surface of sensing material. When the operating temperature increases from 160 to 240 °C, it provides more energy for thermal reactions between ethanol and oxygen species, resulting in the improved sensing properties. However, when the operating temperature keeps rising, the desorption rate of gas molecules exceeds its adsorption rate, which will decrease the amount of ethanol on surfaces of sensing materials. Lower concentration of ethanol molecules would lead to the decreased sensitivity of sensing materials. Therefore, 240 °C is an optimal operating temperature for gas sensing devices based on pure In_2O_3 and $\text{Co}_3\text{O}_4\text{-In}_2\text{O}_3$ heterojunction structure. Besides, the response of pure Co_3O_4 is a little different. The response reaches its maximum at 260 °C.

Co_3O_4 content in composite system is another significant element which should be taken into consideration in gas sensing study. As can be seen from Fig. 4b, the gas response values of pure In_2O_3 , $\text{Co}_3\text{O}_4\text{-In}_2\text{O}_3$ (1 %), $\text{Co}_3\text{O}_4\text{-In}_2\text{O}_3$ (10 %) and pure Co_3O_4 are 45.82, 62.13, 17.54 and 5.36, respectively. As we expected, the response value based on $\text{Co}_3\text{O}_4\text{-In}_2\text{O}_3$ (1 %) is 1.36 times higher than that of pure In_2O_3 . Remarkably, the response value of $\text{Co}_3\text{O}_4\text{-In}_2\text{O}_3$ (1 %) is 11.6 times higher than that of pure Co_3O_4 . The result shows that the synergistic effects make the sensing properties of heterojunction surpass both pure In_2O_3 and Co_3O_4 .

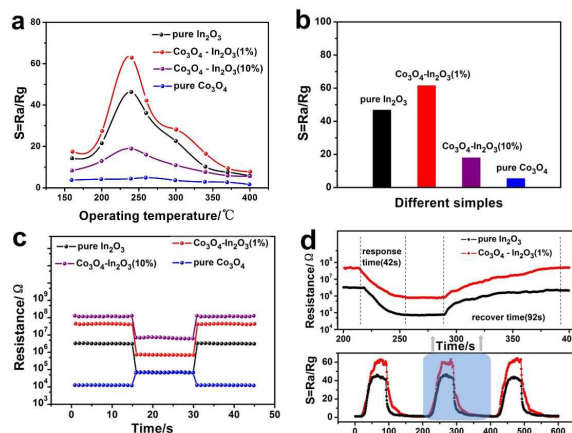


Fig. 4 (a) The response of different samples towards 100 ppm of ethanol operated at different temperatures; (b) The response of samples with different contents of Co_3O_4 towards 100 ppm of ethanol; (c) The resistance curves of samples with different contents of Co_3O_4 towards 100 ppm of ethanol; (d) The response transients of pure In_2O_3 and $\text{Co}_3\text{O}_4\text{-In}_2\text{O}_3$ (1%) gas sensing devices towards 100 ppm of ethanol.

Moreover, the gas response of $\text{Co}_3\text{O}_4\text{-In}_2\text{O}_3$ with other content of Co_3O_4 was exhibited in Fig. S3. Obviously, the response values decrease with the increased Co_3O_4 . This phenomenon can be explained in Fig. 4c, in which the resistance curves of pure In_2O_3 , $\text{Co}_3\text{O}_4\text{-In}_2\text{O}_3$ (1%), $\text{Co}_3\text{O}_4\text{-In}_2\text{O}_3$ (10%) and pure Co_3O_4 towards 100 ppm of ethanol were presented. At first, all sensing devices were exposed to air for 15 s. Obviously, in air atmosphere, the sensing devices based on pure Co_3O_4 exhibit extremely low resistance. In addition, the resistances of $\text{Co}_3\text{O}_4\text{-In}_2\text{O}_3$ composite system increase with the elevated contents of Co_3O_4 . The sharp rise of resistances can be ascribed to the p-n junctions formed between n-type In_2O_3 and p-type Co_3O_4 , and these results are in accordance with the theory of previous literature.⁴² Subsequently, when the ethanol vapor was introduced, the resistances of sensing devices show a decreased trend except the sensing devices based on Co_3O_4 , indicating the characteristic of n-type In_2O_3 and p-type Co_3O_4 semiconductors.^{24, 43} Besides, all kinds of the heterojunction structures show an n-type response, which can be attributed to the high content of n-type In_2O_3 .

For practical application, the gas sensing response and recovery time are also important parameters to evaluate the performance of gas sensors. To simulate practical gas sensing procedure, the response transients of gas sensing devices based on pure In_2O_3 and $\text{Co}_3\text{O}_4\text{-In}_2\text{O}_3$ (1%) towards 100 ppm of ethanol were also studied (Fig. 4d). Measured from the curves, we find that the $\text{Co}_3\text{O}_4\text{-In}_2\text{O}_3$ (1%) heterojunction structure has superior ethanol response value (1.41 times higher than pure In_2O_3 , which is consistent with previous test). Nevertheless, these two kinds of sensing materials show similar response and recovery times. More details can be discovered in the resistance variation curves that obtained by calculating the values of response transients. Apparently, we can figure that the response and recover time of $\text{Co}_3\text{O}_4\text{-In}_2\text{O}_3$

(1%) are 42 and 92 s, respectively, which is relatively high. Now, we are making some further study in order to reduce the response and recover times.

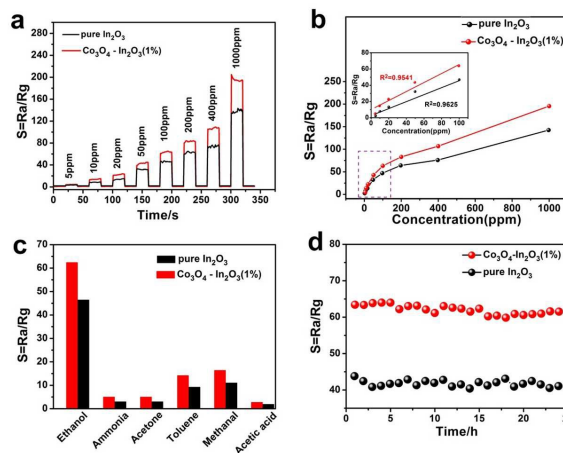


Fig. 5 (a) The response of pure In_2O_3 and $\text{Co}_3\text{O}_4\text{-In}_2\text{O}_3$ (1%) towards ethanol with different concentrations; (b) The sensitivity tendency of pure In_2O_3 and $\text{Co}_3\text{O}_4\text{-In}_2\text{O}_3$ (1%) vs different gas concentrations, and the inset shows corresponding calibration curves (5 to 100 ppm); (c) The response of pure In_2O_3 and $\text{Co}_3\text{O}_4\text{-In}_2\text{O}_3$ (1%) towards 100 ppm of different target gases; (d) The stability test of pure In_2O_3 and $\text{Co}_3\text{O}_4\text{-In}_2\text{O}_3$ (1%) towards 100 ppm of ethanol.

For the sake of investigating gas sensing limitation, the sensing properties of pure In_2O_3 and $\text{Co}_3\text{O}_4\text{-In}_2\text{O}_3$ (1%) gas sensing devices towards 5 to 1000 ppm of ethanol were also performed (Fig. 5a). It is obviously that the response values increase rapidly with increased ethanol concentrations. Besides, the response values of $\text{Co}_3\text{O}_4\text{-In}_2\text{O}_3$ (1%) are significantly higher than those of pure In_2O_3 . Notably, the response value of $\text{Co}_3\text{O}_4\text{-In}_2\text{O}_3$ (1%) to 5 ppm of ethanol is 4.4 (1.43 times higher than pure In_2O_3), indicating the high sensitivity and wide detection range of $\text{Co}_3\text{O}_4\text{-In}_2\text{O}_3$ (1%). To further investigate the sensitivity tendency of obtained samples towards different concentrations of ethanol, the linear fitting method is also performed (Fig. 5b). As we can see, the responses exhibit linear growth process when ethanol vapor concentration increases from 5 to 100 ppm. Moreover, the linear calibration curve (inset of Fig. 5b) further demonstrates that the sensing devices fabricated in this work have good accuracy and reliability.

Fig. 5c presents the selectivity of pure In_2O_3 and $\text{Co}_3\text{O}_4\text{-In}_2\text{O}_3$ (1%) towards ethanol over other VOCs: ammonia, acetone, toluene, methanal, and acetic acid. As these six kinds of gas are very common in our daily life or factories, and the selectivity is important to an ethanol sensing devices.^{44, 45} Apparently, these two gas sensing devices show strongest response to ethanol among different gases with the same concentration (100 ppm), indicating the superior selective ability in gas detection process. Notably, the $\text{Co}_3\text{O}_4\text{-In}_2\text{O}_3$ (1%) exhibits higher response values than those of pure In_2O_3 to all kinds of VOCs, which confirms the universality of $\text{Co}_3\text{O}_4\text{-In}_2\text{O}_3$ (1%) in different gas atmospheres.

When it comes to practical application, the good stability is another important factor that should be taken into consideration. Fig. 5d presents stability tests of pure In_2O_3 and $\text{Co}_3\text{O}_4\text{-In}_2\text{O}_3$ (1 %) towards 100 ppm of ethanol. After these two gas sensing devices continued working for 24 h, no visible decrease in gas response can be observed. This phenomenon indicates the outstanding stability and repeatability of $\text{Co}_3\text{O}_4\text{-In}_2\text{O}_3$ heterojunction. High stability and repeatability mean superior lifetime of gas sensing devices, which is another significant advantage for practical application. What's more, humidity can also affect the response of sensing materials. So we tested our samples in different humidity to simulate the real environment (Fig. S4). The result shows that the responses decrease by 21 % when the humidity changes from 50 to 90 %.

Table 1 compares the response of $\text{Co}_3\text{O}_4\text{-In}_2\text{O}_3$ (1 %) to ethanol with other metal oxide semiconductors. It is evident that $\text{Co}_3\text{O}_4\text{-In}_2\text{O}_3$ (1 %) exhibits higher gas response values and lower optimal operating temperature than those of other different kinds of sensing materials. For example, compared with In_2O_3 hierarchical nanostructures, the response of

samples fabricated in this work is 2.25 times higher and the operating temperature is also lower.

Gas sensing mechanism was also investigated to help explain the enhanced sensing performance of $\text{Co}_3\text{O}_4\text{-In}_2\text{O}_3$ (1 %). For n-type metal oxide semiconductors, just like pure In_2O_3 fabricated in this work, the sensing mechanism has been reported in previous studies.^{46, 47} Firstly, when n-type In_2O_3 semiconductors are exposed in air atmosphere at optimal operating temperature, oxygen molecules would be adsorbed on surfaces of sensing materials and then trap electrons from the conduction band of In_2O_3 to form ionized oxygen species (O_{ads}^- , O_2^- , and O_2^-), leading to the formation of electron depletion layer in surfaces of sensing materials. The resistance of sensing materials would greatly increase, which has been defined as R_a above. Whereafter, when n-type In_2O_3 semiconductors are exposed in target gas, the resistance of sensing materials (R_g) would reduce rapidly, because the reductive molecules can react with ionized oxygen species and give back trapped electrons. The response value of n-type sensing materials can be simply summarized as the change of their resistances in different atmosphere.

Table 1 The comparative analysis of gas sensing response of different materials

Materials	Ethanol (ppm)	Operating temperature(°C)	Gas response	Reference
Co_3O_4 nanorod arrays	500	160	70.7	13
In_2O_3 hierarchical nanostructures	100	320	27.6	17
Bi_2O_3 nanoparticle-decorated In_2O_3 nanorods	200	200	17.7	48
ZnO nanorods	100	320	25.4	49
SnO_2/ZnO hierarchical nanostructures	100	400	6.2	50
$\text{Co}_3\text{O}_4\text{-In}_2\text{O}_3$ heterojunction	100	240	62.13	this work
$\text{Co}_3\text{O}_4\text{-In}_2\text{O}_3$ heterojunction	200	240	82.99	this work

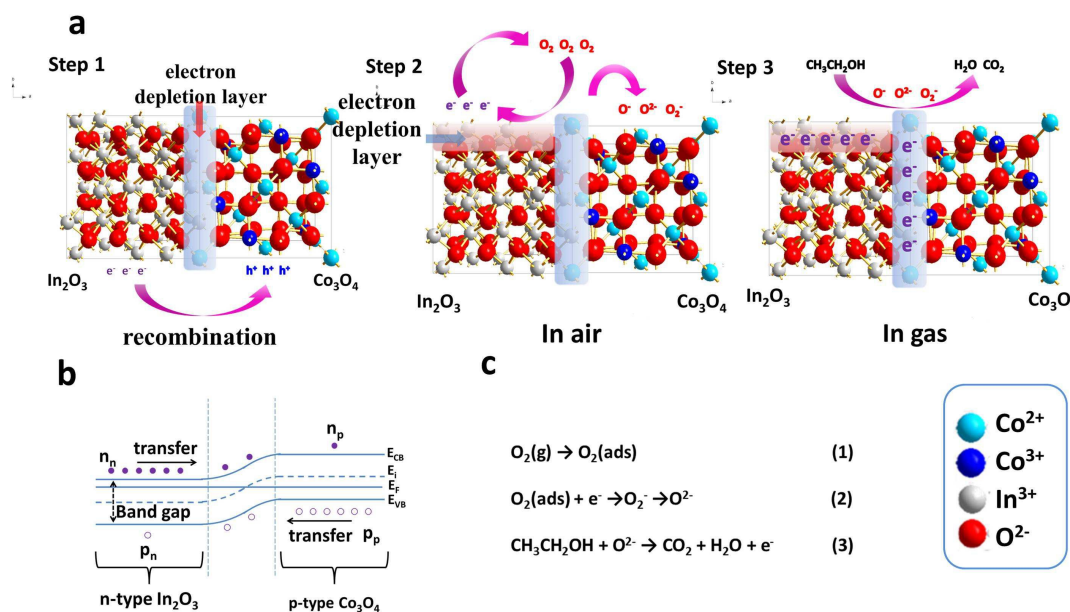


Fig. 6 (a) Schematic illustrations for the gas-sensing mechanism of $\text{Co}_3\text{O}_4\text{-In}_2\text{O}_3$ (1 %); (b) The formation mechanism of electron depletion layer formed at p-n heterojunction structure; (c) Reaction equations of sensing process.

The sensing mechanism of $\text{Co}_3\text{O}_4\text{-In}_2\text{O}_3$ heterojunction structure is somewhat different with n-type In_2O_3 . It is known that electron depletion layer would form at the contact interface between n-type and p-type semiconductors.^{42, 51, 52} Fig. 6b exhibits dynamic process of the formation of electron depletion layer in this work. Firstly, n-type In_2O_3 and p-type Co_3O_4 nanoparticles are combined together tightly through calcination process. As we know, in n-type semiconductors, electrons are the majority carriers (labeled as n_n in Fig. 6b). And yet, in p-type semiconductors, holes are the majority carriers (labeled as p_p in Fig. 6b). So after these two kinds of semiconductors come into contact with each other, it would be easy for electrons transfer from n-type In_2O_3 to p-type Co_3O_4 . Finally, electrons and holes which belongs to p-type Co_3O_4 will recombine at the contact interface, leading to the rapidly reduced concentration of charge carrier and sharply increased resistance compared with pure n-type In_2O_3 . This theory is also in agreement with previous consequence in this work (Fig. 4c). Besides the electron depletion layer showed in step 1 in Fig. 6a, another kind of electron depletion layer would be formed in surfaces of sensing materials operated at optimal temperature (step 2 in Fig. 6a), and the mechanism is similar to pure n-type metal oxide semiconductors. Both the two electron depletion layers contribute to the great improvement of resistance. When ethanol molecules are introduced, they would react with the ionized oxygen species. At this time, the electrons would be released back to In_2O_3 semiconductor and p-n heterojunction through surface interactions (step 3 in Fig. 6a). Therefore, these two kinds of electron depletion layer would disappear gradually. This phenomenon will cause the resistance of sensing devices decrease sharply, which also means higher response values. The reactions in the sensing progress can be seen in Fig. 6c.⁵³ The reactions can further describe the details of gas sensing procedure. Generally, in the presence of heterojunction structure, the gas sensing devices based on $\text{Co}_3\text{O}_4\text{-In}_2\text{O}_3$ (1 %) heterojunction structure have superior sensing performance compared with pure In_2O_3 sensing devices.

Conclusions

In summary, the $\text{Co}_3\text{O}_4\text{-In}_2\text{O}_3$ heterojunction structure was successfully prepared through a simple grinding-calcination process without any harmful agents. Gas sensing devices based on $\text{Co}_3\text{O}_4\text{-In}_2\text{O}_3$ (1 %) heterojunction structure exhibit higher response and selectivity to ethanol compared with pure In_2O_3 . Moreover, $\text{Co}_3\text{O}_4\text{-In}_2\text{O}_3$ (1 %) shows low operating temperature, low detection limitation and high stability, which are significantly important in practical application. This work provides a new idea to fabricate high sensitivity gas sensing devices in a simple, cheap and environmentally friendly method.

Acknowledgements

Kai Song and Xiaoqian Meng contributed equally to this work. This investigation was supported by the Natural Science Foundation of China (No. 51322212, 51472122), the Fundamental Research Funds for the Central Universities (No. 30915011201), the PAPD and "333 project" of Jiangsu.

Notes and references

- R. Ramanathan, S. Walia, A. E. Kandjani, S. Balendran, M. Mohammadtaheri, S. K. Bhargava, K. Kalantar-zadeh and V. Bansal, *Langmuir : the ACS journal of surfaces and colloids*, 2015, **31**, 1581-1587.
- S. Prezioso, F. Perrozzi, L. Giancaterini, C. Cantalini, E. Treossi, V. Palermo, M. Nardone, S. Santucci and L. Ottaviano, *The Journal of Physical Chemistry C*, 2013, **117**, 10683-10690.
- A. Gurlo, *Nanoscale*, 2011, **3**, 154-165.
- D. Chen, J. Xu, Z. Xie and G. Shen, *ACS applied materials & interfaces*, 2011, **3**, 2112-2117.
- X. Chen, Z. Guo, W.-H. Xu, H.-B. Yao, M.-Q. Li, J.-H. Liu, X.-J. Huang and S.-H. Yu, *Advanced Functional Materials*, 2011, **21**, 2049-2056.
- P. Sun, W. Zhao, Y. Cao, Y. Guan, Y. Sun and G. Lu, *CrystEngComm*, 2011, **13**, 3718.
- J. Ding, J. Zhu, P. Yao, J. Li, H. Bi and X. Wang, *Industrial & Engineering Chemistry Research*, 2015, **54**, 8947-8953.
- C. Wang, J. Zhu, S. Liang, H. Bi, Q. Han, X. Liu and X. Wang, *J. Mater. Chem. A*, 2014, **2**, 18635-18643.
- X. Wang, W. Liu, J. Liu, F. Wang, J. Kong, S. Qiu, C. He and L. Luan, *ACS applied materials & interfaces*, 2012, **4**, 817-825.
- S. Elouali, L. G. Bloor, R. Binions, I. P. Parkin, C. J. Carmalt and J. A. Darr, *Langmuir : the ACS journal of surfaces and colloids*, 2012, **28**, 1879-1885.
- T. Wagner, C. D. Kohl, S. Morandi, C. Malagu, N. Donato, M. Latino, G. Neri and M. Tiemann, *Chemistry*, 2012, **18**, 8216-8223.
- Y. Lu, W. Zhan, Y. He, Y. Wang, X. Kong, Q. Kuang, Z. Xie and L. Zheng, *ACS applied materials & interfaces*, 2014, **6**, 4186-4195.
- Z. Wen, L. Zhu, W. Mei, Y. Li, L. Hu, L. Sun, W. Wan and Z. Ye, *Journal of Materials Chemistry A*, 2013, **1**, 7511.
- A. Mirzaei, K. Janghorban, B. Hashemi and G. Neri, *Journal of Nanoparticle Research*, 2015, **17**.
- D. R. Miller, S. A. Akbar and P. A. Morris, *Sensors and Actuators B: Chemical*, 2014, **204**, 250-272.
- N. Singh, R. K. Gupta and P. S. Lee, *ACS applied materials & interfaces*, 2011, **3**, 2246-2252.
- D. Han, P. Song, H. Zhang, H. Yan, Q. Xu, Z. Yang and Q. Wang, *RSC Adv.*, 2014, **4**, 50241-50248.
- S. Wang, P. Wang, Z. Li, C. Xiao, B. Xiao, R. Zhao, T. Yang and M. Zhang, *New J. Chem.*, 2014, **38**, 4879-4884.
- S. Xu, J. Gao, L. Wang, K. Kan, Y. Xie, P. Shen, L. Li and K. Shi, *Nanoscale*, 2015, **7**, 14643-14651.
- X. Hu, X. Zhou, B. Wang, P. Sun, X. Li, C. Wang, J. Liu and G. Lu, *RSC Adv.*, 2015, **5**, 4609-4614.
- S. Kim, S. Park, G.-J. Sun, S. K. Hyun, K.-K. Kim and C. Lee, *Current Applied Physics*, 2015, **15**, 947-952.
- H.-Y. Lai, T.-H. Chen and C.-H. Chen, *CrystEngComm*, 2012, **14**, 5589.

PAPER

RSC Advances

23. P. Song, D. Han, H. Zhang, J. Li, Z. Yang and Q. Wang, *Sensors and Actuators B: Chemical*, 2014, **196**, 434-439.
24. L. Gai, L. Ma, H. Jiang, Y. Ma, Y. Tian and H. Liu, *CrystEngComm*, 2012, **14**, 7479.
25. S. Wang, B. Xiao, T. Yang, P. Wang, C. Xiao, Z. Li, R. Zhao and M. Zhang, *Journal of Materials Chemistry A*, 2014, **2**, 6598.
26. N. Singh, A. Ponzoni, R. K. Gupta, P. S. Lee and E. Comini, *Sensors and Actuators B: Chemical*, 2011, **160**, 1346-1351.
27. Z. Wang, Z. Li, J. Sun, H. Zhang, W. Wang, W. Zheng and C. Wang, *The Journal of Physical Chemistry C*, 2010, **114**, 6100-6105.
28. H. Huang, H. Gong, C. L. Chow, J. Guo, T. J. White, M. S. Tse and O. K. Tan, *Advanced Functional Materials*, 2011, **21**, 2680-2686.
29. J. M. Wu, *Journal of Materials Chemistry*, 2011, **21**, 14048-14055.
30. Y. Lou, J. Ma, X. Cao, L. Wang, Q. Dai, Z. Zhao, Y. Cai, W. Zhan, Y. Guo, P. Hu, G. Lu and Y. Guo, *ACS Catalysis*, 2014, **4**, 4143-4152.
31. Y. Lou, X.-M. Cao, J. Lan, L. Wang, Q. Dai, Y. Guo, J. Ma, Z. Zhao, Y. Guo and P. Hu, *Chemical Communications*, 2014, **50**, 6835-6838.
32. W. Zhang, J. Zhang, M. Zhang, C. Zhang, A. Zhang, Y. Zhou, Y. Tang and P. Wu, *New J. Chem.*, 2015, **39**, 8249-8253.
33. Q. Lu, S. Liu, M. Ren, L. Song and G. Zhao, *Journal of Sol-Gel Science and Technology*, 2011, **61**, 169-174.
34. G. Xi and J. Ye, *Inorganic Chemistry*, 2010, **49**, 2302-2309.
35. W. Li, X. Wu, N. Han, J. Chen, X. Qian, Y. Deng, W. Tang and Y. Chen, *Sensors and Actuators B: Chemical*, 2016, **225**, 158-166.
36. W. Yin, J. Su, M. Cao, C. Ni, S. G. Cloutier, Z. Huang, X. Ma, L. Ren, C. Hu and B. Wei, *The Journal of Physical Chemistry C*, 2009, **113**, 19493-19499.
37. C. Kranert, R. Schmidt-Grund and M. Grundmann, *physica status solidi (RRL) - Rapid Research Letters*, 2014, **8**, 554-559.
38. I. Lorite, J. J. Romero and J. F. Fernández, *Journal of Raman Spectroscopy*, 2012, **43**, 1443-1448.
39. J. Gan, X. Lu, J. Wu, S. Xie, T. Zhai, M. Yu, Z. Zhang, Y. Mao, S. C. Wang, Y. Shen and Y. Tong, *Scientific reports*, 2013, **3**, 1021.
40. C. Yuan, L. Yang, L. Hou, L. Shen, X. Zhang and X. W. Lou, *Energy & Environmental Science*, 2012, **5**, 7883.
41. X. Zhou, W. Feng, C. Wang, X. Hu, X. Li, P. Sun, K. Shimano, N. Yamazoe and G. Lu, *J. Mater. Chem. A*, 2014, **2**, 17683-17690.
42. A. Kargar, Y. Jing, S. J. Kim, C. T. Riley, X. Pan and D. Wang, *ACS nano*, 2013, **7**, 11112-11120.
43. L. Li, M. Liu, S. He and W. Chen, *Analytical chemistry*, 2014, **86**, 7996-8002.
44. N. Lu, X. Gao, C. Yang, F. Xiao, J. Wang and X. Su, *Sensors and Actuators B: Chemical*, 2016, **223**, 743-749.
45. A. Giberti, D. Casotti, G. Cruciani, B. Fabbri, A. Gaiardo, V. Guidi, C. Malagù, G. Zonta and S. Gherardi, *Sensors and Actuators B: Chemical*, 2015, **207**, 504-510.
46. N. Barsan and U. Weimar, *Journal of Electroceramics*, 2001, **7**, 143-167.
47. M. Tiemann, *Chemistry*, 2007, **13**, 8376-8388.
48. S. Park, S. Kim, G. J. Sun and C. Lee, *ACS applied materials & interfaces*, 2015, **7**, 8138-8146.
49. L. Wang, Y. Kang, X. Liu, S. Zhang, W. Huang and S. Wang, *Sensors and Actuators B: Chemical*, 2012, **162**, 237-243.
50. N. D. Khoang, D. D. Trung, N. Van Duy, N. D. Hoa and N. Van Hieu, *Sensors and Actuators B: Chemical*, 2012, **174**, 594-601.
51. L. Wang, Y. Kang, Y. Wang, B. Zhu, S. Zhang, W. Huang and S. Wang, *Materials Science and Engineering: C*, 2012, **32**, 2079-2085.
52. S. Park, S. Kim, H. Kheel and C. Lee, *Sensors and Actuators B: Chemical*, 2016, **222**, 1193-1200.
53. C. Zhao, G. Zhang, W. Han, J. Fu, Y. He, Z. Zhang and E. Xie, *CrystEngComm*, 2013, **15**, 6491.